1   **Equivalency Points: Predicting Concrete Compressive Strength Evolution in Three Days**

2

3

4   M. Viviani[a*] B. Glisic[b], K.L. Scrivener[c], I. F.C. Smith[d]

5

6

7   ---

8   [a] GCC Technology and Processes, Yverdon-les-Bains, Switzerland

9   [b] Smartec SA, Manno, Switzerland

10   [c] Ecole Polytechnique Fédérale de Lausanne (EPFL), Laboratoire des matériaux de construction (LMC)

11   [d] Ecole Polytechnique Fédérale de Lausanne (EPFL), Laboratoire d'informatique et de mécanique

12   appliquées à la construction (IMAC)

13   ---

14

15

16   **ABSTRACT**

17

18

19   Knowledge of the compressive strength evolution of concrete is critical for activities such as stripping

20   formwork, construction scheduling and pre-stressing operations. Although there are several procedures

21   for predicting concrete compressive strength, reliable methodologies involve either extensive testing or

22   voluminous databases. This paper presents a simple and efficient procedure to predict concrete strength

23   evolution. The procedure uses an experimentally-determined parameter called the *Equivalency Point* as

*Corresponding author: Marco Viviani, Av. des Sciences 1/A, Yverdon les Bains, Switzerland.
Email : mviviani@gcc.com

an indicator of equivalent degree of reaction. Equivalency Points are based on early age concrete

deformation and temperature variations. Test results from specimens made from seven concrete types

validate the approach.

1 INTRODUCTION

A maturity method is used to predict the compressive strength evolution of concrete. Timely

knowledge of such evolution helps to schedule operations such as pre-stressing and removal of

formwork. The speed of construction can thus be increased using maturity methods without

endangering safety. Such knowledge can also contribute to quality control. For example, the durability

of structures is increased by avoiding excessive loading at early age.

The progress of hydration can be expressed by the degree of reaction α, expressed as the percent of the

total product of reaction developed at a given time.

Maturity methods use functions of time and temperature to compute the progress of the hardening

reactions. Semi-empirical formulas link the progress of reaction to strength. Values for the activation

energy (E_a) and the rate of reaction (k) are necessary to implement the maturity approach when

46   equivalent time [1] is used as a function to calculate the progress of the hardening reaction.

47   Determination of these values usually requires either extensive testing or large databases. In this paper,

48   a simple and fast methodology to determine the activation energy E_a, the rate of reaction k_r (rate of

49   reaction at a reference temperature T_r) and to predict compressive strength evolution is presented. This

50   method also includes the determination of two other mixture-specific parameters necessary to model

51   the evolution of compressive strength - the time at start of strength development (Et_0) and the ultimate

52   compressive strength (S_u), strength at time t=∞.

53   The Arrhenius equation can be used to determine the rate of a reaction when the value for activation

54   energy, Ea, and a frequency factor, A, is known [2]. In order to reduce the number of unknowns, an

55   alternative to the direct use of Arrhenius equation has been proposed. This is the maturity or Equivalent

56   time (Et) (see Equation 1, [1]). Et is the integral in time of the ratio between the rates of reaction $k = k$

57   (T) and $k_r = k(T_r)$ of two specimens of the same concrete type that are hardening at different

58   temperatures. One is a virtual reference specimen that is assumed to be kept at a constant temperature

59   T_r (generally 20 °C in Europe; 23 °C in USA). The other specimen is real and has a varying

60   temperature T. R is the gas constant.

61
$$Et(t, T) = \int_{t_0}^{t} \left[\exp - \frac{Ea}{R} \left(\frac{1}{T} - \frac{1}{T_r} \right) \right] dt \quad Eq.1$$

62   The equivalent time is of great interest for prediction of properties it allows comparison of concrete

63   specimens that are hydrating at different rates. Among the formulas that link strength and equivalent

64   time, the following semi-empirical relation is the most used. Equation 2 employs k_r and Et to predict

65   the compressive strength [3].

66
$$S(k_r, Et) = S_u \frac{k_r (Et - Et_0)}{1 + k_r (Et - Et_0)} \quad Eq.2$$

67

68   Carino and Lew have used successfully used this model for estimation of the 28-days strength [3]. To

69   compute Et for a concrete, knowledge of the activation energy, E_a, is necessary (see Equation 1).

70   Furthermore, to predict strength using Equation 2, k_r, Et_0 and S_u must also be known.

71

72   This paper describes a new methodology to determine E_a and k_r using early age measurements of

73   deformations, temperatures and strengths. A methodology is also given for the determination of the

74   parameters S_u and Et_0 in Equation 2, [5, 4]. These values are then used to predict the strength evolution

75   in seven types of concrete covering a broad range of mix designs used in practice. The errors arising

76   are analysed and a sensitivity analysis of the strength prediction is done for different values of the

77   activation energy and the number of calibration points.

78

79

80   **2 MEASUREMENT SYSTEM**

81

82   Optical-fiber deformation sensors can be regarded as extensometers. They measure the deformation of

83   the host material between the extremities of the gauge. They can be applied on the external surface of a

84   structural member, as well as embedded in the material. Fiber optic sensors may have long or short

85   gauge length. In general, Fabry-Perot and Michelson types are long gauge (>250 mm gauge length),

86   while Bragg-grating types are short gauge (gauge length of few millimeters). All types can measure

87   static and dynamic deformations. A long-gauge fiber-optic deformation sensor has recently been

88   developed to measure deformation in fresh in concrete without being perturbed by the moisture of the

89   host material, temperature changes or magnetic fields [6]. The measurement system of the sensor is

90   based on low coherence interferometry using single-mode optical fibers. The system includes a reading

91   unit and fiber optic sensors. Figure 1 shows the system schematically. The reading unit is composed of

92   a light emitter (LED), a low-coherence Michelson interferometer, completed with the optical devices

93   used to carry, filter and analyze the light beams. The sensor consists of two single-mode optical fibers

94   (called *measurement* and *reference* fiber). The measurement fiber is rigidly connected with the two

95   anchor pieces and prestressed by 0.5%. Thus, it is able to follow the changes of length between the

96   anchor pieces, both in traction and in compression. The stiffness of the sensor can be changed using

97   stiffer or softer protection pipes. The reference fiber is glued to the anchor pieces but loose inside the

98   protection tube (see Figure 2), hence the movement of the anchor pieces will not produce any changes

99   of reference fiber length. Both fibers have, at one extremity, chemically deposed mirrors (see Figure 2).

100   One of the two fibers is slightly shorter than the other, in order to create an "initial" interference path.

101

102   The Infrared light emitted by the LED passes through the optical fiber to the sensor, split (normally

103   50%-50%) by the coupler. The light moves along the reference and measurement fiber and is reflected

104   by the mirrors, returning to the reading unit. Here the light generates an interference figure (see Figure

105   3) composed by a central and two lateral peaks.

106

107   This interference figure is analyzed (compensated) by the mobile mirror, and then sent to the PC. When

108   no-deformation is imposed to the sensors, a fringe called "zero"-peak appears. The "zero" interference

109   figure is created by the initial difference of length between the two fibres. When a deformation of the

110   sensor occurs, the two lateral peaks displace, according to the change of the measurement fibre length

111   (see Figure 3). Performing the measurement takes less than 10 seconds. This sensor is particularly

112   suitable for concrete, because of its robustness, temperature compensation, insensitivity to magnetic

113   fields, and a precision of 2 μm. Moreover, such sensors can follow the deformation of fresh concrete

114   without disturbing the strain field of the host material [7]. The stiffness and the thermal expansion

115   coefficient (TEC) of the sensors are influenced mainly by the characteristics of the protective tube.

116

117   Glisic proposed a Michelson sensor called a "setting" sensor with a high axial stiffness because it was

118   housed in a tube made of stainless steel [7, 8]. In this work a "soft sensor" and "stiff sensor" were used,

119   which are Michelson sensors packaged into a soft plastic pipe (soft sensor) and in a steel pipe (stiff

120   sensor) respectively. The different types of packaging (casing) provide a different axial stiffness of the

121   sensors. The soft sensor has a very low stiffness because it is housed in a soft plastic tube and for this

122   reason the soft sensor measures the deformations of the concrete matrix from very early times, as soon

123   as the stiffness of the concrete specimen overtakes the sensor stiffness. The Stiff sensor is similar to

124   the setting sensor or Glisic [7,8], differing only in the type of pipe used and the assembly system. The

125   assemblage of Stiff and Soft sensors is shown in Figure 4. Soft and Stiff sensors have equal gauge

126   length

127

128   The stiff sensor, once embedded in concrete, together with a soft sensor of the same gauge length, leads

129   to determination of a difference curve between the deformation measured by the two sensors. When

130   concrete is placed, the soft sensor measures the swelling (or contraction) of the concrete (because it is

131   very soft) while the stiff sensor is initially not influenced by the deformations of the concrete matrix

132   and therefore the difference between deformations measured by the two sensors increases and then

133 decreases [4]. When the difference becomes constant, this is called the "hardening point" and in a

134 previous article [5] this alone was used to predict 3-day strengths.

135

136 In this paper, the methodology is made more versatile by dividing the difference between the sensors

137 by the variation in temperature in order to account for measurement bias due to temperature; as the

138 shape of the difference curve is dependent on the temperature variation–time history. These curves

139 always show a steep increase and then level off to a constant value (see Figure 5). Later, as the delta

140 temperature or deformation approaches zero there is a vertical asymptote. The point at which a line

141 drawn on the plateau of the $\frac{\Delta \varepsilon_{st-soft}}{\Delta T}$ curve departs from the curve on the left side is defined as the

142 *equivalency point*. This point on the curve is assumed to occur at the same α (degree of reaction) and is

143 the basic assumption of this method for calculating activation energies.

144

145

146 **3 EXPERIMENTAL AND CALCULATION**

147

148 **3.1 Determination of the activation energy** E_a

149

150 The strategy adopted for determining the activation energy uses two specimens of the same concrete. It

151 is based on the determination of the equivalency point of these two specimens. Both specimens have

152 the same dimensions. They are both monitored with a stiff and a soft sensor. Each pair of sensors has

153 the same features. One specimen is wrapped with glass wool. The glass wool acts as insulation and

154   keeps the temperature of this specimen at a higher level than the temperature of the other specimen.

155   The rate of reaction in the insulated cylinder is therefore higher. The temperature is measured in both

156   specimens (see Figure 6). The specimens are cured under sealed conditions – no moisture exchange

157   with the environment. The degree of reaction, in terms of equivalent time (Et), can be calculated by

158   Equation 1. For the specimens under sealed conditions the deformation of the concrete, ε_{conc}, is the

159   sum of the autogenous (ε_{aut}) and thermal (ε_{th}) deformations:

160
$$\varepsilon_{conc} = \varepsilon_{aut} + \varepsilon_{th} = \varepsilon_{aut} + TEC_c * \Delta T \quad Eq.3$$

161   The soft sensor measures the deformation of the concrete matrix from very early age because of its low

162   axial stiffness [7, 8]. It is assumed that the stiff sensor measures a part of the deformation of concrete

163   that is a function of the degree of reaction [7]. So the dependence of the deformation of the stiff sensor

164   on the degree of reaction is expressed by a transfer coefficient $\aleph = \aleph(\alpha)$ which accounts for the

165   percentage of deformation that the interface transfers to the sensor. Thus, the deformation transferred

166   from the concrete to the stiff sensor, $\varepsilon_{conc \rightarrow st}$ can be expressed as follows:

167
$$\varepsilon_{conc \rightarrow st} = \aleph * (\varepsilon_{conc}) \quad Eq.4$$

168   However, the stiff sensor also changes its length according to the thermal expansion coefficient of the

169   casing (steel in this case), TEC_s and to the temperature change (see Figure 7):

170
$$\varepsilon_{steel} = TEC_s * \Delta T \quad Eq.5$$

171   Because the stiff sensor and the hardening material have different and (in the case of concrete)

172   changing thermal expansion coefficients, the changing temperature produces additional differences in

173   deformation, termed here thermal interaction deformation ε_{ti}. This thermal interaction deformation is

174 proportional to the difference of thermal expansion coefficients of the two materials (steel and

175 concrete), K. This effect is also influenced by the transfer coefficient. Thus, this deformation is

176 measured by the stiff sensor with a magnitude proportional to the transfer function $\aleph = \aleph(\alpha)$:

177
$$\varepsilon_{ti \to st} = \aleph * (K * \Delta T) \quad \text{Eq. 6}$$

178 Therefore, the total deformation measured by the stiff sensor is the sum of the terms in Equations 4-6:

179
$$\varepsilon_{st} = \aleph * (K * \Delta T + \varepsilon_{aut} + TEC_c * \Delta T) + TEC_s * \Delta T \quad \text{Eq. 7}$$

180 The difference between the deformation measured by the soft and the stiff sensor is determined by

181 Equation 9:

182
$$\begin{cases} \varepsilon_{soft} \approx \varepsilon_{conc} = \varepsilon_{aut} + TEC_c * \Delta T \\ \varepsilon_{st} = \aleph * K * \Delta T + \aleph * \varepsilon_{aut} + \aleph * TEC_c * \Delta T + TEC_s * \Delta T \end{cases} \quad \text{Eq. 8}$$

183
$$\Delta \varepsilon_{st\text{-}soft} = \aleph * K * \Delta T + (\aleph - 1) * \varepsilon_{aut} + (\aleph - 1) * TEC_c * \Delta T + TEC_s * \Delta T \quad \text{Eq. 9}$$

184 In Equation 9, the term $\Delta \varepsilon_{st\text{-}soft}$ (t) is the hardening curve [4]. Dividing both sides of Equation 9 by ΔT

185 the following equation is obtained:

186
$$\frac{\Delta \varepsilon_{st\text{-}soft}}{\Delta T} = \aleph * K + \frac{(\aleph - 1)}{\Delta T} * \varepsilon_{end} + (\aleph - 1) * TEC_c + TEC_s \quad \text{Eq.10}$$

187 It is assumed that at a certain degree of reaction ($\alpha = \alpha^*$) – the *Equivalency Point* – the deformation is

188 fully transferred to the stiff sensor (non slip point), i.e. that $\aleph(\alpha*) = 1$, in which case equation 10

189 becomes:

9

190
$$\frac{\Delta\varepsilon_{\text{st-soft}}}{\Delta T} = K + TEC_s \qquad \text{Eq. 11}$$

191 In Equation 11 the value of $\frac{\Delta\varepsilon_{\text{st-soft}}}{\Delta T}$ becomes a constant when K becomes constant. Since the thermal

192 expansion coefficient of steel is constant in time, the coefficient K is constant when the thermal

193 expansion coefficient of the hardening material is constant. When K is constant Equation 11 describes

194 a horizontal line on a plot of $\frac{\Delta\varepsilon_{\text{st-soft}}}{\Delta T}$ versus time. A further analysis of Equation 11 indicates the

195 possible shapes of the experimental curves. Two situations might occur:

196
$$\begin{array}{l} \Delta\varepsilon_{\text{st-soft}} \neq 0 \\ \Delta T \neq 0 \\ \aleph = 1 \end{array} \quad \rightarrow \text{the curve will level off to a constant value}$$

197
$$\begin{array}{l} \Delta\varepsilon_{\text{st-soft}} = 0 \\ \Delta T = 0 \\ \aleph = 1 \end{array} \quad \rightarrow \text{a vertical asymptote will appear}$$

198 The two situations are shown in Figure 5.

199

200 The *Equivalency Point* occurs at a constant degree of reaction for the same hardening material. This

201 assumption is valid under two conditions. The first is that $\aleph = \aleph(\alpha)$; i.e. the interfacial bond strength, is

202 a function of the degree of reaction. This assumption is supported by the literature which indicates that

203 the characteristics of interfaces between bars or fibers and cement-based materials evolve with the

204 degree of reaction [9, 10, 11]. The second assumption is that K (or the TEC of concrete) becomes

205 constant. Few results have been found concerning the evolution of thermal expansion coefficient of

206 concrete in term of degree of reaction [12, 13, 14, 5, 15]. However many researchers agree to define

207   the TEC_c as a function of the degree of reaction. The Equivalency Point usually appears in the first

208   10–30 hours of equivalent time, in the zone where $\Delta\varepsilon \neq 0; \Delta T \neq 0$.

209

210   The definition of Equivalency Point can be used to extract the activation energy E_a from hardening

211   measurements. If two specimens of the same concrete are monitored with stiff, soft and temperature

212   sensors but with different temperature regimes (Figure 8), the equivalency point can be determined for

213   each specimen. For both specimens the Equivalency Point occurs at the same equivalent time

214   (maturity). Temperature profiles are inserted in Equation 1 for each specimen and the integral is

215   calculated to the Equivalency Point. This results in two equations with two unknown values (Et and E_a)

216   which can be solved. The values are shown in Table 1.

217

218   **3.2 Determination of the zero equivalent time**

219   The Zero equivalent time, Et_0 in Equation 2 is the time at which strength development starts.

220   Conventionally this could be taken as the setting time, but as the setting time is somewhat arbitrary and

221   would require separate measurement; here we take it as the point when the self heating of the concrete

222   starts, which is equivalent to the start of the acceleration of hydration leading to hardening. This point

223   can be extracted from the data acquired during the tests, by study of the temperature curves. Before the

224   hydration reaction starts to accelerate the temperature of the concrete is influenced by the ambient

225   temperature. During this period three situations may occur depending on the temperature difference

226   between the mixed concrete and its surroundings.

227   a.   Heating;

228   b.   Constant temperature; and

229   c.   Cooling.

230   Situation (a) is very unlikely and was never seen in this work, but Et_0 can in any case be detected from

231   the upturn of the temperature curve (case 1, Figure 9). In Situation (b) Et_0 can also be detected when

232   the temperature shows a sharp increase (case 2, Figure 9). The third situation is the most difficult.

233   Cooling occurs as a consequence of lower external temperature and can be assumed to be linear in the

234   first hours. The moment when fast hydration begins was therefore taken as the moment when the

235   temperature curve loses its linearity (see Case 3 in Figure 9). This methodology is directly related to

236   what occurs in each pour of concrete and was found to be more relevant than determining the setting

237   time at a reference temperature and taking this as the Et_0 for all the pours of the same concrete. This

238   method avoids the need for separate measurements and also allows the effect of chemicals (such as

239   plasticizers) on the rate of reaction to be taken into account. Results for the 7 concretes studied are

240   reported in Table 1

241

242   **3.3 Determination of Su and k_r.**

243

244   Quantification of the activation energy is necessary but not sufficient for predicting strength. The

245   prediction of the compressive strength evolution is possible if two calibration compressive strength

246   tests are conducted at different Equivalent times using standard specimens of the same composition,

247   humidity, boundary conditions and known temperature histories. This allows the values of k_r and Su to

248   be determined. In this article these two calibration strength tests are indicated on the graphs. Values

249   for Su and k_r can be obtained using strength tests at any time; in this work the Calibration tests were

250   carried out at 48 hours and 72 hours after casting. The Equivalent age at the time of the calibration tests

251   was evaluated using the activation energy determined as described in Section 3.1 and the temperature

252   history of the specimen. The zero equivalent time is obtained using the methodology described in

253   Section 3.2. For the two tests the strength, the equivalent time and the zero equivalent time are inserted

254   in Equation 2. This gives two equations which can be solved for the two unknowns (k_r and Su). To

255   further verify the results further calibration strength tests can be used to obtain multiple values for k_r

256   and Su. The new or average values for k_r and Su can be used for a new prediction. Every strength test

257   can be a used as an additional calibration point. In this study the 7-days strength was used as a third

258   calibration test for the analysis of errors. The 24-hour test was not been found to be an appropriate

259   calibration test this may be because the concretes have a 24-hour strengths under standard condition

260   that is close to the lower limit of the testing range and so more variable.

261   **3.4 Tests**

262   Activation energies, k_r, Su and Et_0 were evaluated and applied to seven different types of concrete

263   detailed in Table 2 using the procedure presented above. Five were commonly used concrete types in

264   civil engineering. They were made with different types of aggregate. Air entrainers, superplasticizers

265   and different types of cement (see Table 2). The predicted strength evolution curves shown in Figures

266   10-16 were obtained from calibration strengths obtained within the first 72 hours. The predictions

267   obtained were compared to the criteria given by the Texas Department of Transportation code (TEX-

268   426-A, see Table 3) which was the most stringent found in the literature. They were found to be

269   realistic and acceptable without any correction according to this criteria (see Tables 3 and 4). The

270   quality of the prediction was verified after 7, 21 and 28 days (with exception of Test 7, for which test at

271   21 days is not available). Times of strength testing were 2, 3, 7, 21 and 28 days actual elapsed time and

272   not equivalent time. The maximum deviation between predicted and tested values of each test is

273   presented in Table 4. A comparison with values determined with the earlier method using hardening

274   times [5] show that the results are essentially similar, but with slightly lower maximum error (6.2 % in

275   comparison to 7.4%). It is also important to note that this method based on the determination of

276   equivalency points is faster and more automated evaluation of the activation energy than determination

277   of hardening times.

278

279

280   **3.4 Estimation of errors**

281

282   Values for equivalent time are determined using equivalency points (see section 3.1). Equivalency

283   points are determined using measurement of temperature and deformation. Errors affecting

284   measurement thus affect values for activation energy and subsequently, strength predictions.

285   Measurement errors have been estimated for deformation and temperature using experimental values.

286   Measurement noise when reading deformation and temperature as well as time dependent drift are

287   especially important when deformation and temperature readings are added, subtracted multiplied or

288   divided since errors can amplify to become high percentages of results that are reported. Propagation of

289   errors has been estimated in order construct the error envelope for TEC (and for autogenous

290   deformation). The error, Δs, for addition and subtraction of quantities A and B is calculated as follows:

291                              $$\Delta s = \sqrt{\Delta A^2 + \Delta B^2} \quad \text{Eq.12}$$

292   Where:

293   Δs= error related to results of addition or subtraction of quantities A and B

294   ΔA= error related to measuring quantity A

295   ΔB= error related to measuring quantity B

296   For multiplication and division of quantities A and B the error is calculated as follows:

297
$$\Delta r = \sqrt{\left(\frac{\Delta A}{A}\right)^2 + \left(\frac{\Delta B}{B}\right)^2} \quad \text{Eq.13}$$

298   Δr= error related to results of multiplication or division of the quantities A and B

299   The equivalency point is assumed to relate to a certain degree of reaction. This assumption is made on

300   the basis of the mechanism of deformation transferring between the hardening material and sensors.

301   This means that at the equivalency point, the degree of reaction is the same for all specimens of the

302   same material, hydrating in autogenous conditions. This equivalency is independent of the combination

303   of time and temperature that has lead to such a degree of reaction.

304

305   Determination of E_a requires detection of the equivalency point. Errors in the determination of the

306   equivalency point might result in poor predictions of activation energy. Drift and noise related to

307   measurements introduce an error in terms of time on the equivalency point. The worst case scenario for

308   the calculation of the activation energy corresponds to a bound of $\pm$ 6 minutes on values for the

309   equivalency points. This leads to two values for bounds on the activation energy. The worst case

310   scenario on the value for the activation energy has been considered. The variation of the activation

311   energy has an effect on values calculated for strength evolution. The effect of the activation energy

312   variation in strength is shown in Table 5 for predictions made using two calibration times and Table 6

313   for prediction made using three calibrations times (2, 3 and 7 day strengths). Tables 5 and 6 show that,

314   despite propagation of the errors on measurements, prediction fits in all cases the requirements for

315   prediction of code TEX 426 A (except Test 1, two calibration times, upper bound E_a value). These

316   show the robustness of the methodology.

317

318

4 DISCUSSION

320

321 The methodology presented here assumes that the Equivalency Point is an indicator of the degree of

322 reaction. The good predictions obtained support this assumption for the range of concretes studied.

323 Constraints on the testing procedure (such as minimum difference in temperature profiles) could be

324 added for a better definition of hardening time where necessary. The relationship between the

325 hardening curve and the degree of reaction is an important issue for the extension of the methodology

326 to the general field of hardening materials and this will be the subject of further study. The basis of the

327 proposed methodology allows the thermodynamic-chemical properties (activation energy and rate of

328 reaction) to be determined and converted to compressive strength via calibration tests. Codified

329 methods use similar concepts by inserting the final setting time into maturity-strength equations and

330 performing regression analyses.

331

332

333 Currently, maturity methods are still rarely used in practice. This lack of acceptance is partially related

334 to limited practical experience and the extensive prior testing needed for calibration of classical

335 methods. Confidence in the methodology presented here would be increased through performing more

336 compressive tests during the early age of concrete. For example, using a given pair of compressive-

337 strength values, the value of k_r and Su are obtained, and a predictive curve can be calculated. Using

338 other pairs, an envelope of curves is obtained. A standard apparatus for the application of this

339 methodology is under development. Since the apparatus is reusable and robust, an inexpensive and in-

340 situ application of the methodology is feasible.

341

342

343 **5 SUMMARY AND CONCLUSIONS**

344

345

346 Compressive strengths of several widely used concrete mixes have been successfully predicted using a

347 procedure that involves early age deformation monitoring. The procedure has also been applied to a

348 special concrete in order to study the applicability of the methodology to other types of hardening

349 materials. This methodology allows a fast and accurate prediction of values for compressive strength

350 on site. Common methods for estimation of in place strength requires extensive use of curing of mortar

351 cubes at constant temperatures or the use of databases containing a large number of compressive

352 strength values made at many ages and cured at different temperatures. These databases have to be fed

353 with a statistical relevant number of data before a reliable estimation of the strength can be made.

354 Furthermore all of these methods requires many hours of lab and field time for testing, collecting and

355 analyzing data. The method here allows strength to be *predicted* from concrete monitored in situ and

356 early calibration strengths of test specimens from the same batch of concrete – i.e no prior testing is

357 necessary. All the data can be obtained from specimens cast at the same time and from the same batch

358 as the concrete used on site. Seventy-two hours are sufficient to gather data and predict strength

359 evolution with less than 7% error. Common maturity methods cannot estimate the 28-day strength of a

360 mixture without having a prior set of data on 28-day strength of such mix. The new methodology,

361 presented here based on equivalency points is more flexible and gives lower errors compared to the

362   previously presented method based on hardening time [5]. The method also provides explicit values for

363   the activation energy and the rate of reaction.

364

365

366   **6 ACKNOWLEDGEMENTS**

367

368

372
373
374   **7 NOTATION**
375
376   α Degree of reaction (% of the total product of the reaction)
377   k   Reaction rate h^{-1}
378   k_r Rate of reaction at the reference temperature T_r
379   R Gas constant ($KJ*mole^{-1}* K^{-1}$)
380   T Temperature (K)
381   T_r Reference temperature (K)
382   ΔT change in temperature.
383   Et_0 Equivalent time at start of strength development (hours)
384   Et Equivalent time (hours)
385   S Compressive strength at age t (MPa),
386   S_u Ultimate compressive strength (strength at time t=∞),
387   t Time (hours)
388   t_0 Age at start of strength development (hours)
389   ε_{conc} concrete deformation;
390   ε_{soft} soft sensor deformation;
391   ε_{st} stiff sensor deformation;
392   ε_{aut} concrete autogenous deformation;
393   ε_{steel} steel deformation;
394    $\varepsilon_{conc \rightarrow st}$ deformation transferred from the concrete to the stiff sensor;
395    $\varepsilon_{r \rightarrow st}$ thermal interaction deformation transferred from concrete to stiff sensor; and
396    $\aleph$ Function dependent on the degree of reaction;

397   TEC_c concrete thermal expansion coefficient;
398   TEC_s steel thermal expansion coefficient; and
399   K   constant depending on steel and concrete TEC
400   E_a Activation energy (KJ/mole)
401   A Frequency factor (s^{-1})
402
403
404

8 REFERENCES

406

407 [1] Freiesleben Hansen, P. and Pedersen J., Maturity computer for controlled curing and hardening of
408 concrete, Nordisk Betong, 1 (1977), 19-34.

409

410 [2] Arrhenius, S., On the reaction velocity of the inversion of cane sugar by acids, Zeitschrift für
411 Physikalische Chemie 4 (1889), 226-232. [as translated and published in Margaret H. Back & Keith J.
412 Laidler, 1967, "Selected Readings in Chemical Kinetics" Pergamon, Oxford 1967]

413

414 [3] Carino N.J. and Lew H.S., The maturity method: from theory to application, Proceedings of the
415 2001 Structures Congress & Exposition, Washington, D.C., ASCE, Reston, Virginia, Peter C. Chang,
416 Editor, (2001), 19 p.

417

418 [4] Viviani, M., Monitoring and modeling of construction materials during hardening, Doctoral Thesis
419 No. 3168, EPFL, Lausanne, Switzerland, 2005, 172 p.

420

421 [5] Viviani, M., Glisic, B. and Smith, I. F.C., Three-day prediction of concrete compressive strength
422 evolution, ACI materials J. 102 (4) (2005) 231-236.

423

424 [6] Inaudi, D., Fiber optic sensor network for the monitoring of civil engineering structures, Ph.D.
425 Thesis No. 1612, EPFL, Lausanne, Switzerland, 1997.

426

427 [7] Glisic, B., Fibre optic sensors and behaviour in concrete at early age, Ph.D. Thesis, N°2186, EPFL,
428 Lausanne, Switzerland, 2000.

429

430 [8] Glisic B., Simon N., Monitoring of concrete at very early age using stiff SOFO® sensor, Cement
431 and Concrete Composite 22 (2) (2000) 115-119.

432

433 [9] Chan Y., Li V., Age effect on the characteristics of fibre/cement interfacial properties, Journal of
434 Materials Science 32 (19) 1997, 5287-5292.

435

436 [10] Holshemacher, K., Weisse, D., Klotz, S., Bond of reinforcement in ultra high strength concrete,
437 proceedings, International symposium on ultra high performance concrete, September 13-15, Kassel,
438 Germany, 2004, pp. 375-387.

439

440 [11] Delatte, N. J., Fowler, D. W. and Williamson, M. S., Bond strength development with maturity of
441 high-early-strength bonded concrete overlays, ACI Materials J. 97 (2) 2000 201-207.

442

443 [12] Turcry P., Loukil A., Barcelo L. and Casabonne J. M., Can the maturity concept be used to
444 separate the autogenous shrinkage and thermal deformation of a cement paste at early age?, Cement
445 and Concrete Research 32 (9) 2002 1443–1450.

447 [13] Laplante P., Boulay C., Evolution du coefficient de dilatation thermique du béton en fonction de
448 sa maturité aux tout premiers âges, Materials and Structures 27 1994 596-605

450 [14] Bjøntegaard, Ø., Thermal dilation and autogenous deformation as driving forces to self-induced
451 stresses in high performance concrete, Ph.D. Thesis, The Norwegian University of Science and
452 Technology, N-7491 Trondheim, Norway, 1999.

454 [15] Bjøntegaard, Ø., Sellevold E., Interaction between thermal dilation and autogenous deformation in
455 high performance concrete, Materials and Structures 34 2001 266-272.
456

9 FIGURES and TABLES

458   **Table 1, Values for t_0, Ea, k_r, S_u and E_t at the equivalency point for the 7 types of concretes**
459   **studied.**

Test number	Initial time t0 (h)	Ea J/mol	k_r h^{-1}	S_u MPa	Et at the equivalency point, (hours at 20°C)
Test 1	2.7	39000	.0147	43.0	14.45
Test 2	2.2	28100	.0441	37.9	25.3
Test 3	4.0	27000	.0198	51.0	18.1
Test 4	2.5	42600	.0090	46.9	15.55
Test 5	0	36600	.0213	35.7	15.75
Test 6	22.75	25500	.0321	182.8	49.85
Test 7	1.25	36500	.0289	53.5	13.4

460

461

462   **Table 2 Mix-design test 1-7**

	Test 1	Test 2	Test 3	Test 4	Test 5	Test 6	Test 7
Water/cement Ratio	0.45	0.45	0.48	0.48	0.48	0.18	0.43
Cement type	CEM II / A-LL 42.5 R	CEM I 42.5 R	CEM I 42,5 N HS	CEM III/A 32,5 N	CEM II/ A-LL 32.5 R	CEM I 52,5 N HTS	-
Cement	325 Kg/m3	350 Kg/m3	360 Kg/m3	360 Kg/m3	360 Kg/m3	1051.1 Kg/m3	420 Kg/m3
Superplasticizer	0.9%	0.8%	0.8%	0.8%	0.8%	35.1 kg/m^3	No
Air Entrainer	0.1%	-	-	-	-	-	-
Aggregate	0-32 Hüttwangen	0-32 Sergey	0-32 Sergey	0-32 Sergey	0-32 Sergey	0-4 Sand of Fontainebleau	0-32 Sergey
Silica fume	-	-	-	-	-	273.3 Kg/m^3	No
Steel fibre	-	-	-	-	-	Yes*	No
Max. temperature difference	5 °C	15 °C	20.2 °C	14.5 °C	21.6 °C	14.5 °C	30 °C

463
464

465 **Table 3 Verification criteria for maturity prediction; code TEX-426-A. s = predicted strength, s***
466 **= independent test results.**

Verification criteria	Adjusting procedure
$s^* \leq 0.90\ s$ $s^* \geq 1.10\ s$	Develop new S-M relationship
3 consecutives within $0.90\ s \leq s^* \leq 0.95\ s$ $1.05\ s \leq s^* \leq 1.10\ s$	Evaluate batching and placement adjust s-M relationship if needed
Better correlations	S-M relationship accepted

467

468

469 **Table 4 Maximum error between predicted strength and independent test results for the**
470 **methodology proposed in this paper (equivalency points) and for a previous proposal using**
471 **hardening times [4]**

Maximum Errors

Test	Day of occurrence of max. error	Maximum error % (equivalency points)	Day of occurrence of max. error	Maximum error % (hardening times)
1	21	**+6.2 %**	7	+4.5 %
2	28	-6.0 %	28	-5.1 %
3	28	+5.8 %	28	+5.1 %
4	21	-6.1 %	21	**-7.4 %**
5	28	-5.1 %	28	-6.4 %
6	30	+3.8 %	13	+3.7 %
7	28	+1.3%	8	-

472

473

474 **Table 5 Effect of the variation of the activation energy on the predicted strength (two calibration**
475 **points)**

Test number		Activation energy J/mol	k_r h^{-1}	S_u MPa	$\dfrac{\text{Predicted strength - Average test strength}}{\text{Average test strength}} \bullet 100$		
					7th day	21st day	28th day
Test 1	+	53250	.0162	41.2	-6.5	-3.5	-10.2
	mid	39000	.0147	43.0	-5.4	-1.0	-6.2
	-	28200	.0158	41.4	-4.5	0.8	-3.6
Test 2	+	37400	.0393	38.3	4.1	3.4	5.3
	mid	28100	.0441	37.9	4.4	4.1	6.0
	-	20600	.0483	40.0	4.6	4.6	6.6
Test 3	+	31500	.0202	50.7	-1.7	0.3	-5.3
	mid	27000	.0198	51.0	-1.9	-.2	-5.8
	-	23300	.0195	51.2	-2.0	-0.4	-6.1
Test 4	+	48800	.0090	47.8	1.3	5.1	1.9
	mid	42600	.0090	46.9	1.3	6.1	3.2
	-	36900	.0090	46.1	1.3	7.0	4.3
Test 5	+	40000	.0209	35.9	-1.5	0.9	4.7
	mid	36600	.0213	35.7	1.3	1.2	5.1
	-	26000	.0204	36.2	0.9	0.5	4.2
Test 6	+	27900	.0312	183.8	-4.1	-2.3	0
	mid	25500	.0321	182.8	-3.8	-1.9	.4
	-	24000	.0326	182.1	-3.6	-1.7	.7
Test 7	+	53450	.0253	55.0	.6	-	-2.1
	mid	36500	.0289	53.5	1.3	-	-.2
	-	24000	.0317	52.6	2.1	-	1.2

476

477 **Table 6 Effect of the variation of the activation energy on the predicted strength (three**
478 **calibration points)**

Test number	Activation energy J/mol		k_r h^{-1}	S_u MPa	$\dfrac{\text{Predicted strength - Average test strength}}{\text{Average test strength}} \bullet 100$	
					21st day	28th day
	+	53250	.0162	41.2	-.7	-4.3
Test 1	mid	39000	.0173	39.8	1.8	-1.3
	-	28200	.0181	38.9	3.4	0.7
	+	37400	.0339	40.2	0.3	1.8
Test 2	mid	28100	.0377	39.9	.4	2.1
	-	20600	.0409	39.7	.5	2.3
	+	31500	.0208	50.1	1.2	-4.3
Test 3	mid	27000	.0209	50	1.4	-4.1
	-	23300	.0212	49.8	1.6	-3.8
	+	48800	.0086	49.4	2.8	-.7
Test 4	mid	42600	.0086	48.5	3.9	.7
	-	36900	.0090	47.7	4.9	1.9
	+	40000	.0202	36.2	.5	4.3
Test 5	mid	36600	.0204	36.1	.7	4.5
	-	26000	.0199	36.3	.3	4.1
	+	27900	.0355	177.1	.7	3.1
Test 6	mid	25500	.0361	176.6	.8	3.3
	-	24000	.0365	176.3	.9	3.4
	+	53450	.0248	55.4	-	-2.8
Test 7	mid	36500	.0276	54.4	-	-1.5
	-	24000	.0296	53.9	-	.9

479
480
481
482
483

25

484
485
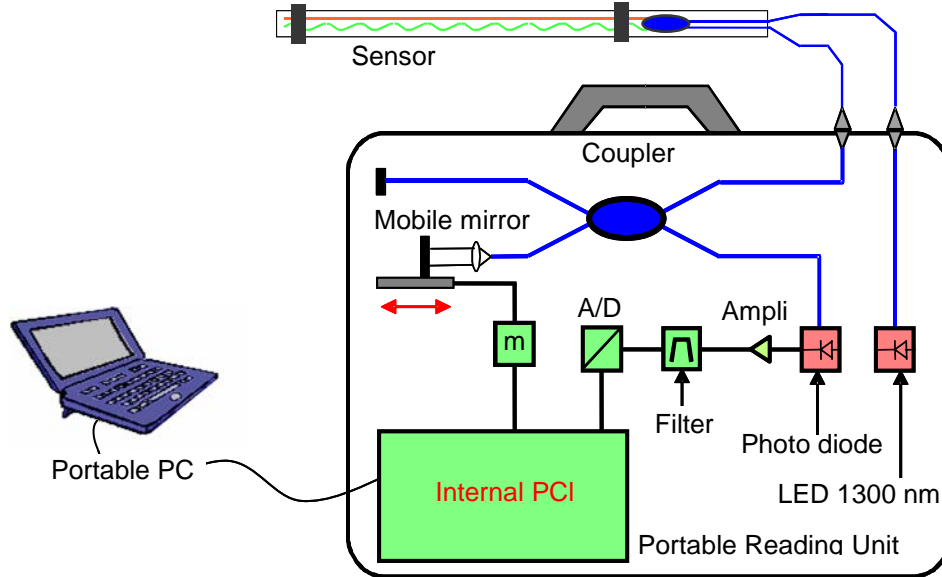
Figure 1 The SOFO monitoring system set-up

486
487
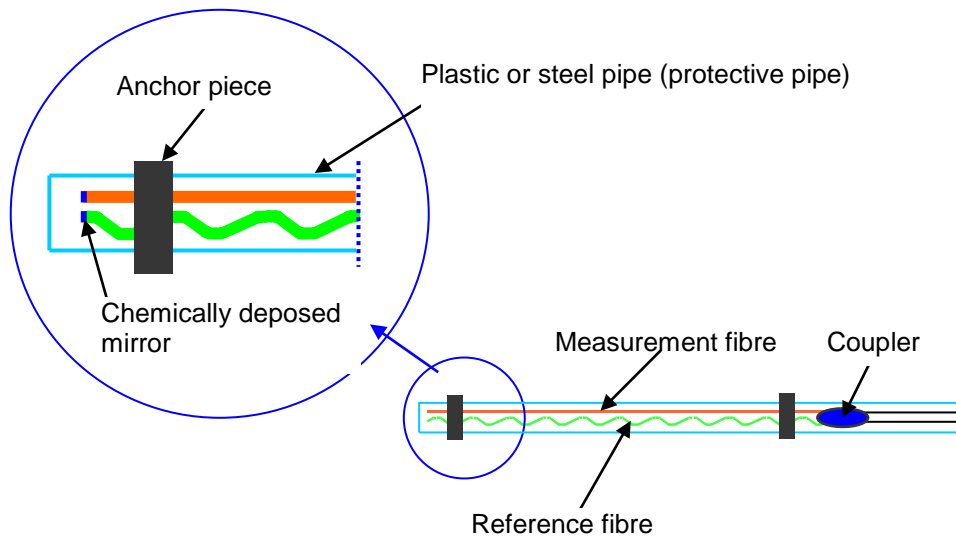
Figure 2 A general scheme of the SOFO sensor

488

Central Peak

Lateral Peaks

a)

c

Length Difference between Measurement
and Reference Fibre

Actual measurement peak

Peak of the "Zero"
Measurement

b)

c

Deformation of the sensor
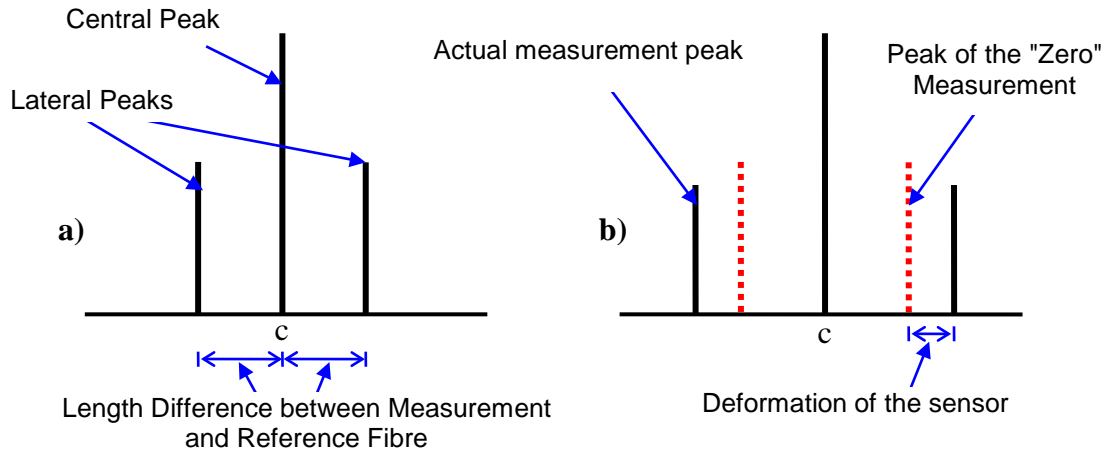
Figure 3 A scheme of the SOFO measurement representation
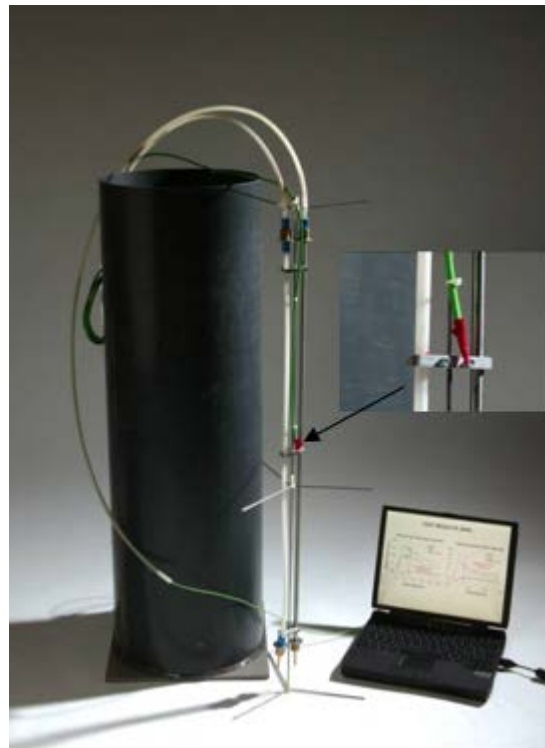
Figure 4 The soft and stiff SOFO sensors. [3]
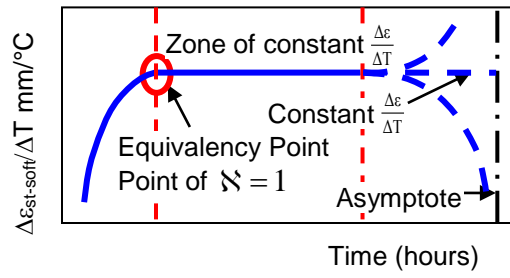
Figure 5 Predicted shape of the $\dfrac{\Delta\varepsilon_{\text{st-soft}}}{\Delta T}$ curve
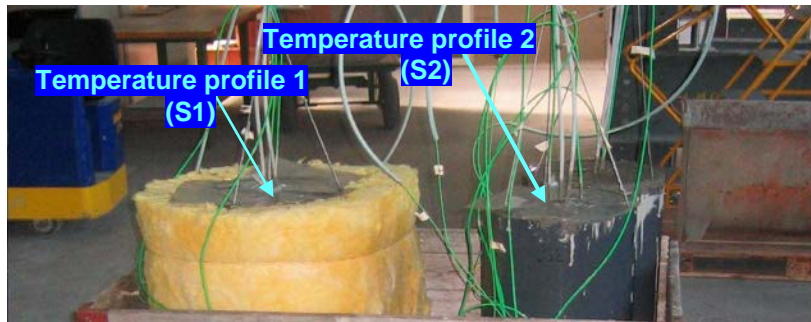
Figure 6 Specimens under test

Figure 7 Reaction deformation

Same reactants, humidity and boundary conditions; two temperature histories

Specimen S1

Stiff Sensor — Soft Sensor

Temperature / Time

Deformation / Time
- Stiff
- Soft

Specimen S2

Stiff Sensor — Soft Sensor

Temperature / Time

Deformation / Time
- Stiff
- Soft

$\dfrac{\Delta\varepsilon_{st-soft}}{\Delta T}$

Equivalency Points

Equivalency curves

Time

$$Et_1 = \int_{t_0}^{t_1}\left[\exp\frac{-E_a}{R}\left(\frac{1}{T_{S1}}-\frac{1}{T_r}\right)\right]dt \quad = \quad Et_2 = \int_{t_0}^{t_2}\left[\exp\frac{-E_a}{R}\left(\frac{1}{T_{S2}}-\frac{1}{T_r}\right)\right]dt$$
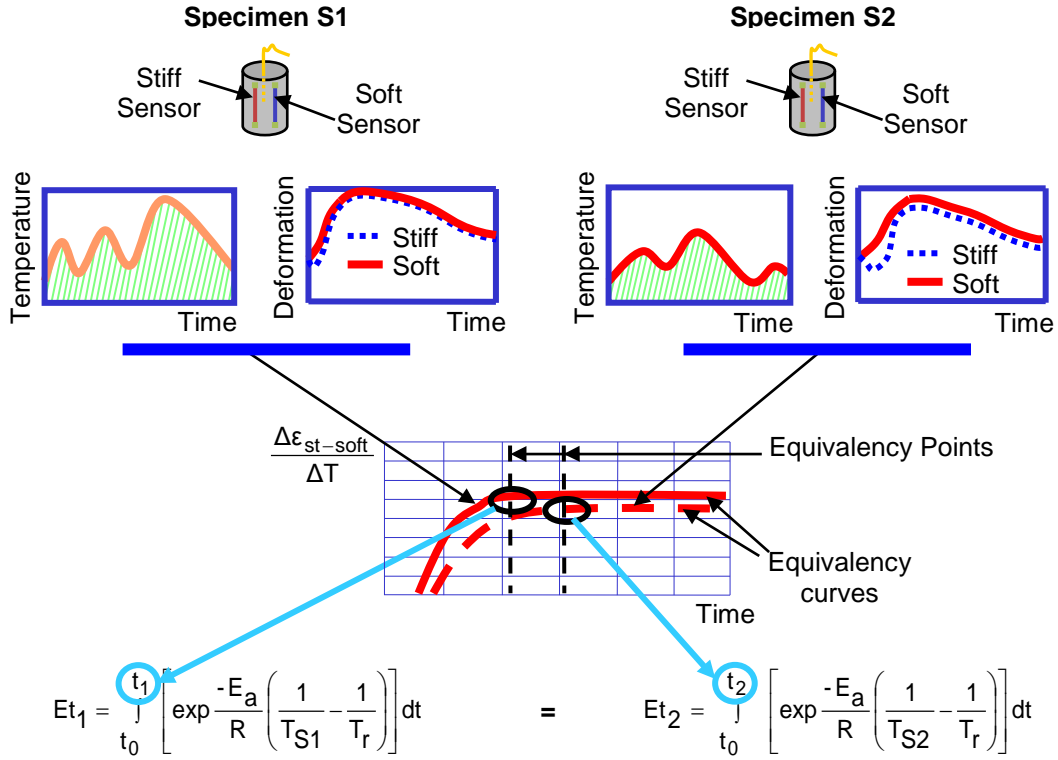
503
504   **Figure 8 Determination of the activation energy E_a**
505
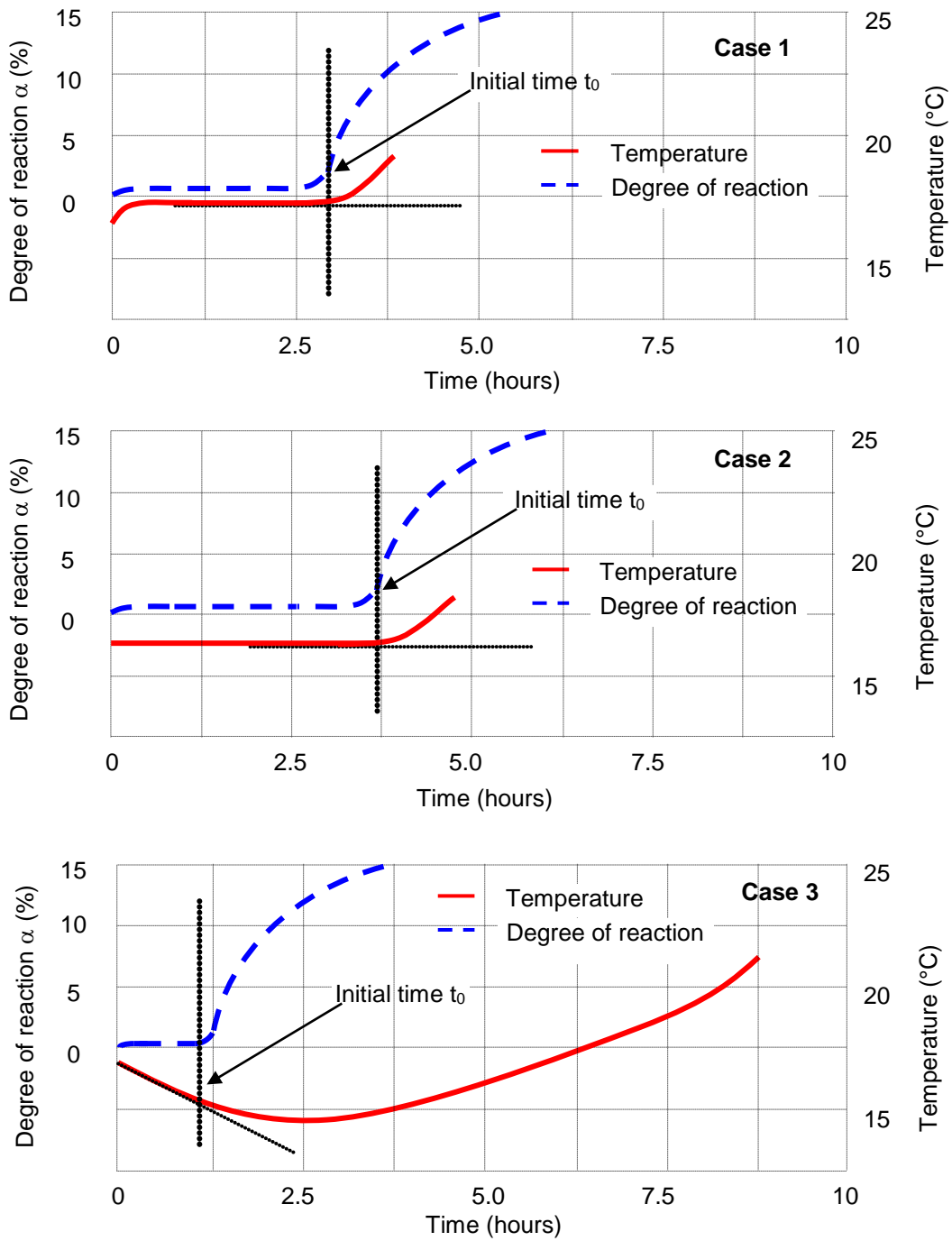
Figure 9 Determination of the time of the Determination of the zero equivalent time
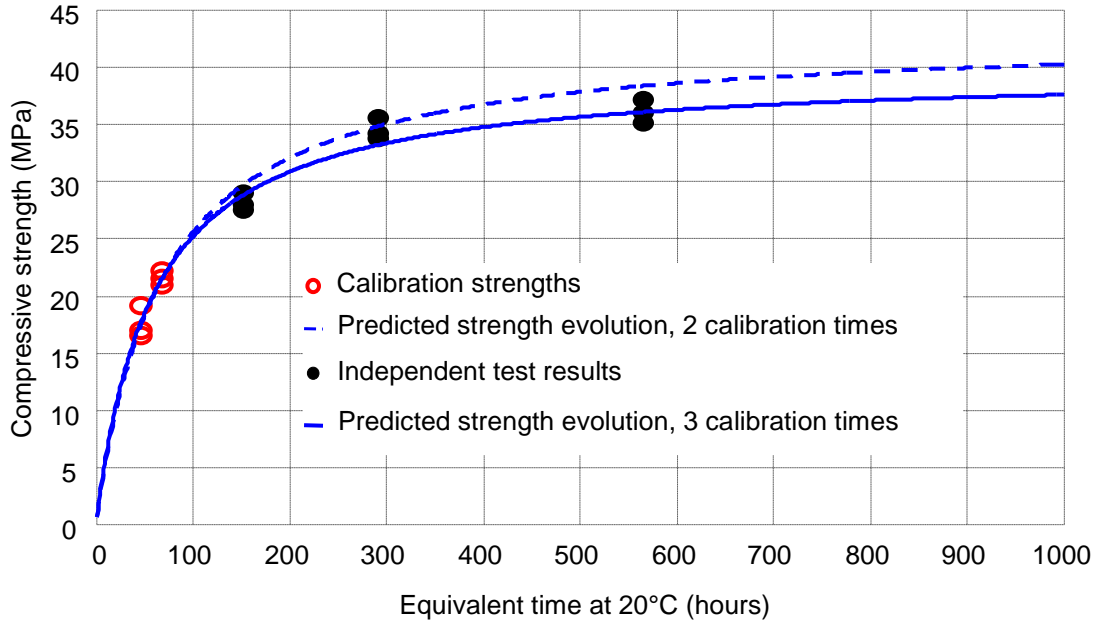
511
Figure 10 Compressive strength vs. equivalent time for test series 1. Calibration strengths of young concrete are used to predict strength evolution and this prediction is verified by independent test results using cylinders containing more mature concrete.
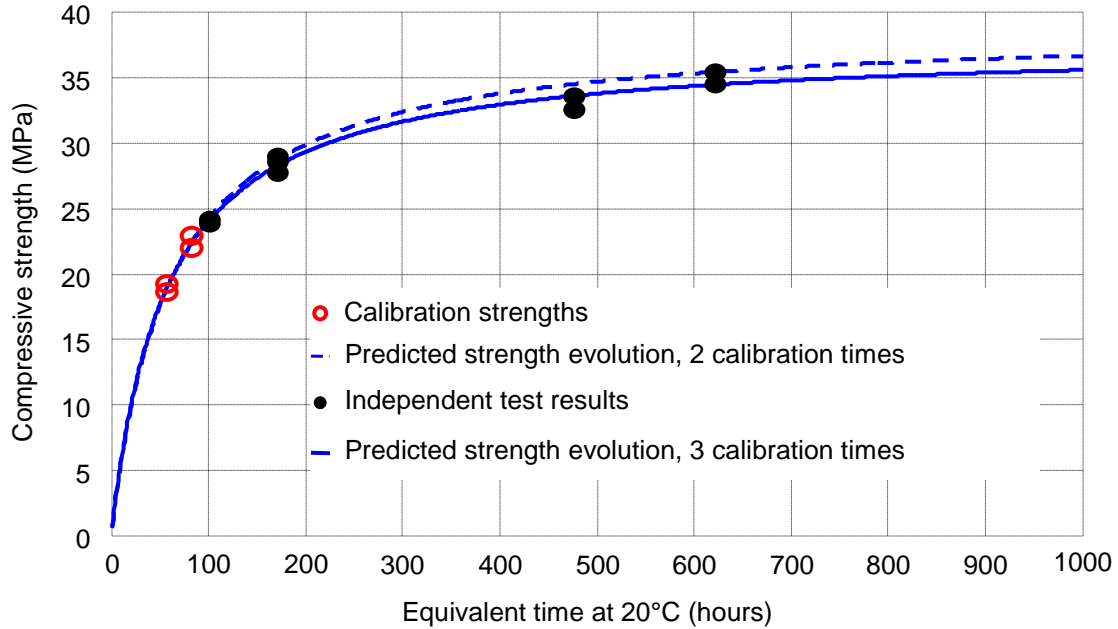
515
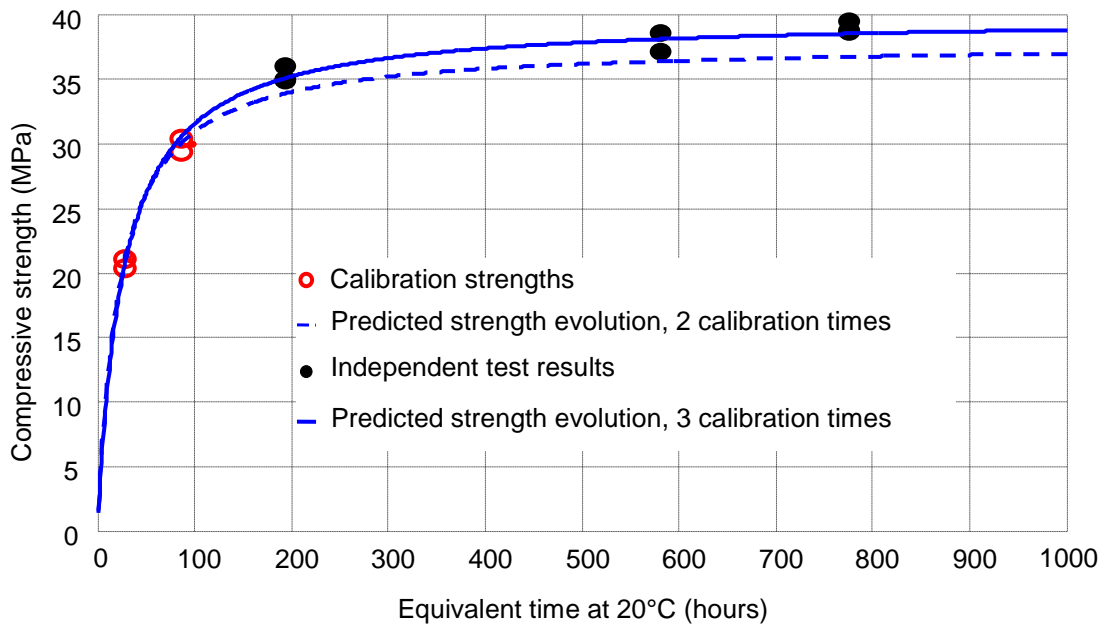
516
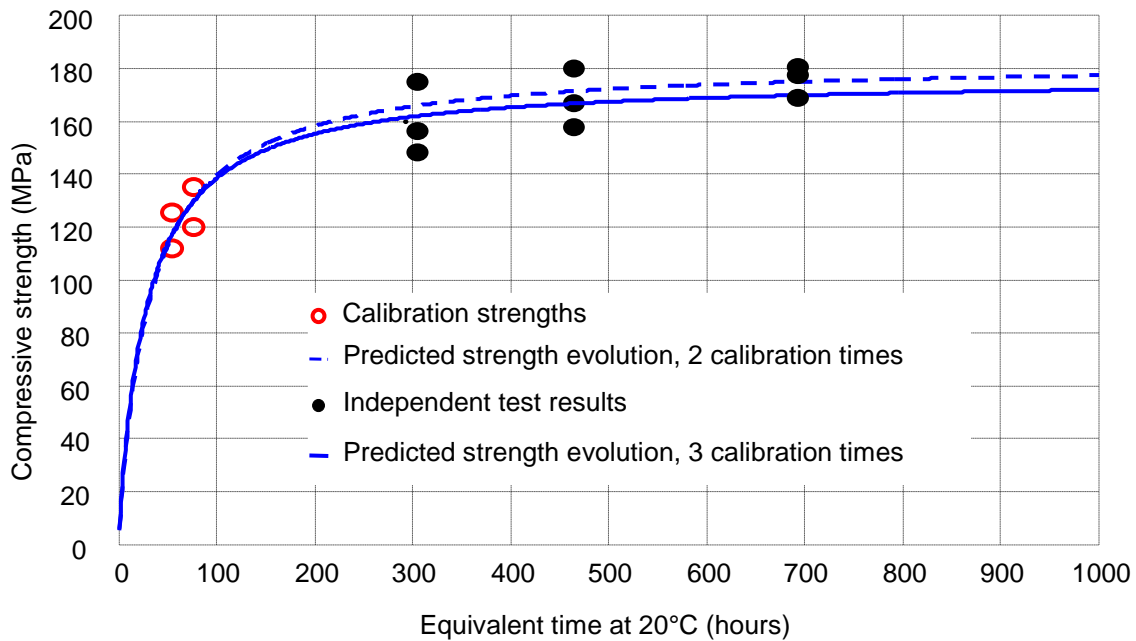**Figure 11 Compressive strength vs. equivalent time for test series 2. Calibration strengths of young concrete are used to predict strength evolution and this prediction is verified by independent test results using cylinders containing more mature concrete.**

520
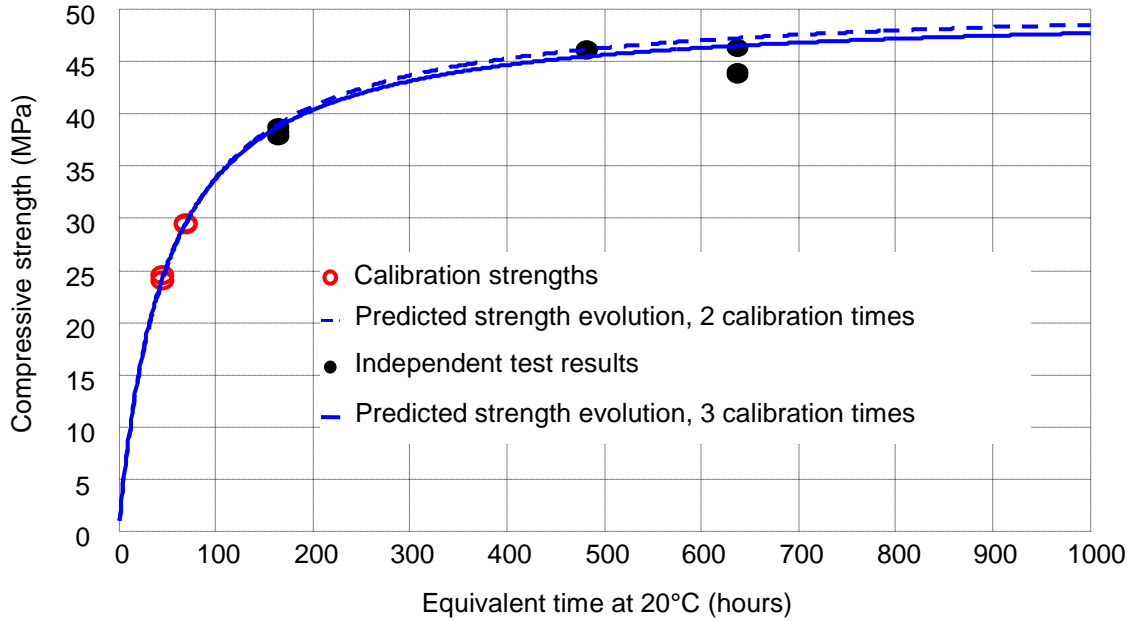
Figure 12 Compressive strength vs. equivalent time for test series 3. Calibration strengths of young concrete are used to predict strength evolution and this prediction is verified by independent test results using cylinders containing more mature concrete.
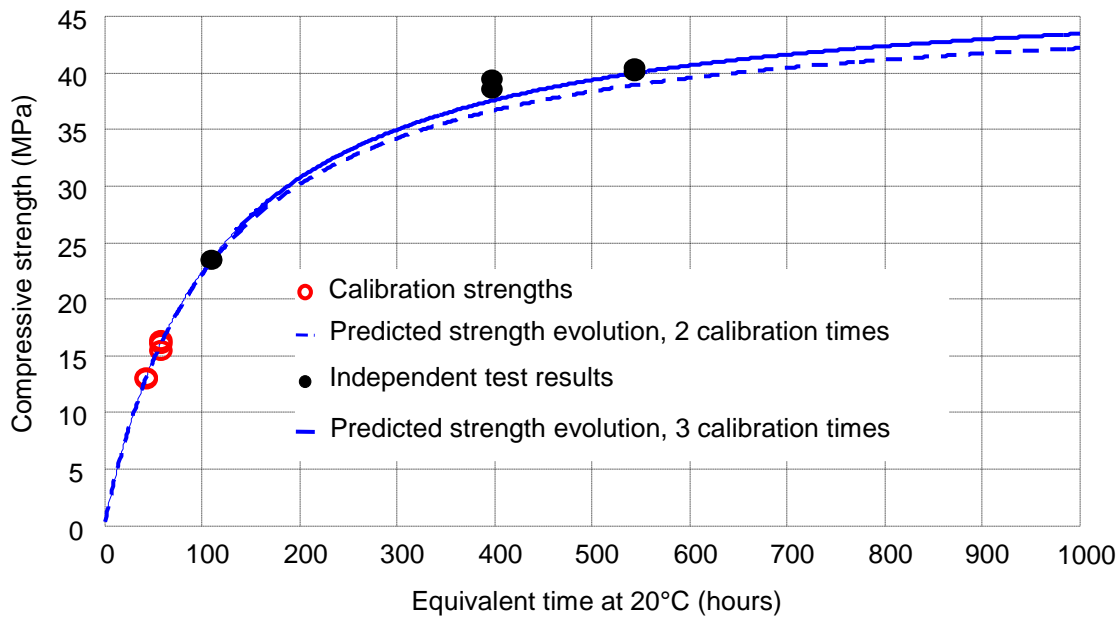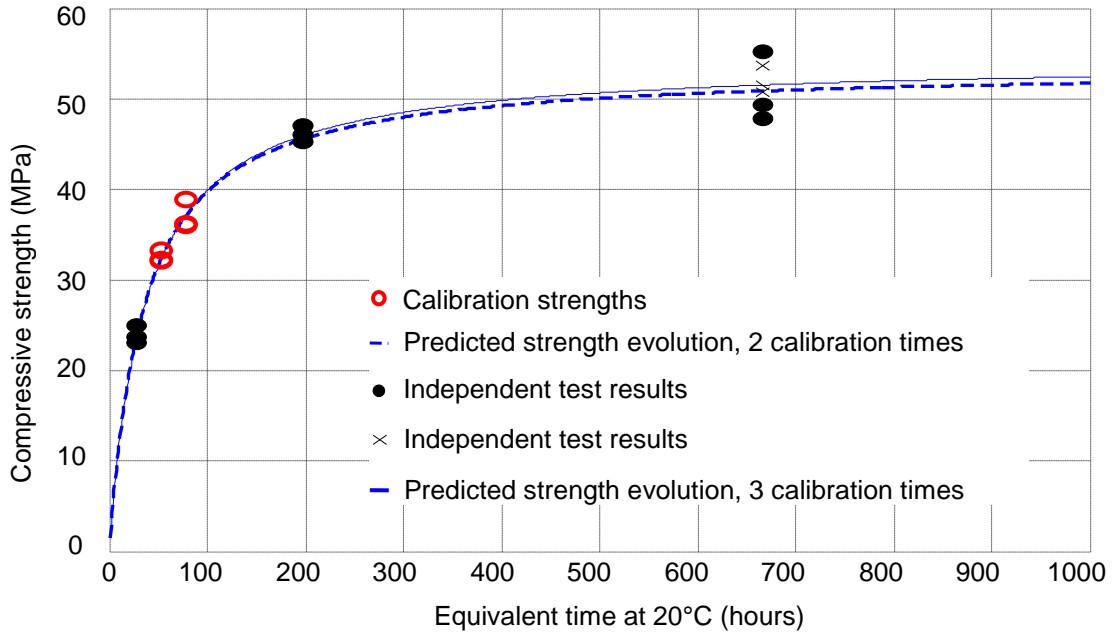

Figure 13 Compressive strength vs. equivalent time for test series 4. Calibration strengths of young concrete are used to predict strength evolution and this prediction is verified by independent test results using cylinders containing more mature concrete.

532
533 **Figure 14 Compressive strength vs. equivalent time for test series 5. Calibration strengths of**
534 **young concrete are used to predict strength evolution and this prediction is verified by**
535 **independent test results using cylinders containing more mature concrete.**
536
537

538
539 **Figure 15 Compressive strength vs. equivalent time for test series 6. Calibration strengths of**
540 **young concrete are used to predict strength evolution and this prediction is verified by**
541 **independent test results using cylinders containing more mature concrete.**
542
543

Figure 16 Compressive strength vs. equivalent time for test series 7. Calibration strengths of young concrete are used to predict strength evolution and this prediction is verified by independent test results using cylinders containing more mature concrete.